Modeling the influence of horizontal advection, deformation, and late uplift on the drainage development in the India-Asia collision zone

Kurt Stüwe,[1] Jörg Robl,[1] Stefan Hergarten,[1] and Lynn Evans[1]

Received 12 July 2007; revised 2 September 2008; accepted 16 September 2008; published 16 December 2008.

[1] We present results of a new model in which we couple a mechanical model to describe continental indentation in plan view with a landscape evolution model to describe drainage development. We apply the model to investigate aspects of the development of drainage systems, erosion, and exhumation in the India-Asia collision zone. It is shown that the orogen-scale distribution of erosion and exhumation can be well matched by the model. However, the elevation of the Tibetan Plateau and the steep topographic gradients at its margins are difficult to reproduce. They appear to require an additional cause of uplift. We show that some of the major observed river capture events can be reproduced by invoking such a late uplift in much of the orogen, except the region of the Sichuan Basin. This includes the inferred capture of the Yarlong-Tsangpo by the Brahmaputra and that of the Upper Yangtze by the Lower Yangtze (thereby deserting the Red River). **Citation:** Stüwe, K., J. Robl, S. Hergarten, and L. Evans (2008), Modeling the influence of horizontal advection, deformation, and late uplift on the drainage development in the India-Asia collision zone, *Tectonics*, *27*, TC6011, doi:10.1029/2007TC002186.

1. Introduction

[2] Landscape evolution models typically consider short- and long-range transport processes during erosion and describe those on two horizontal coordinates [e.g., *Braun and Sambridge*, 1997]. The third dimension, elevation, is evaluated as a variable that is decreased by the erosion model or increased by an independent uplift function. However, few landscape evolution models determine this distribution of uplift dynamically from horizontal shortening or consider lateral advection of drainages due to deformation-driven displacement (although see *Willett et al.* [1999] and *Miller et al.* [2002]). Here we present a numerical model that couples a two-dimensional mechanical model to describe crustal thickening and surface uplift due to continental collision in plan view, with a simple landscape evolution model to describe erosion. We use the model to investigate the resulting drainage development as a function of the evolving topographic gradients.

[3] We apply our model here to a geometry akin to the India-Asia collision zone which displays a spectacular interplay between (1) erosion-driven exhumation [e.g., *Zeitler et al.*, 2001], (2) erosion-driven surface uplift [e.g., *Montgomery and Stolar*, 2006], and (3) horizontal displacement of drainages due to collision, in particular in the region of the syntaxes [e.g., *Hallet and Molnar*, 2001]. Importantly, there is an active debate around a late uplift event that may or may not have affected the region: while some authors have shown that the high elevation of the Tibetan Plateau is at least 35 Ma old [e.g., *Rowley and Currie*, 2006], others have shown that, at least along the eastern margin of the Plateau, the elevated topography appears to be much younger [e.g., *Clark et al.*, 2005a]. Then, this uplift may not be directly related to the uplift caused by the collision. As an alternative, this late uplift has been interpreted as the consequence of tectonics, removal of the mantle lithosphere [*England and Houseman*, 1988], or by lower crustal channel flow [*Clark and Royden*, 2000], but the geometry and timing of this event is as yet very sparsely defined. Recently, several studies have used the major rivers in the orogen to constrain this late uplift on the basis of drainage geometry, incision rates, and capture events [*Clark et al.*, 2004, 2005a; *Schoenbohm et al.*, 2006b]. Our study aims to constrain the geometry of this late uplift on the basis of the observed river capture events using a numerical model.

2. Geological Background

[4] India originally collided with Asia some 50–55 Ma ago and has since indented the Asian plate over a length of some 3,000 km [*Hodges*, 2000, and references therein]. Since the original collision, about 2,500 km of convergence has occurred and is still continuing at a rate of several centimeters per year [*Lee and Lawver*, 1995; *Zhang et al.*, 2004]. Because of the long time span of the continuing convergence between the two plates, *Molnar and Lyon-Caen* [1988] initially suggested that the Tibetan Plateau was caused by successive widening and northward propagation of the zone of crustal thickening and elevated topography due to deformation. Since, a series of field investigations have documented that the uplift history of the Tibetan Plateau is not continuous [e.g., *Harrison et al.*, 1992; *Tapponnier et al.*, 2001] and that Cenozoic shortening structures are missing in substantial parts of the eastern

[1]Department of Earth Science, University of Graz, Graz, Austria.

0278-7407/08/2007TC002186$12.00

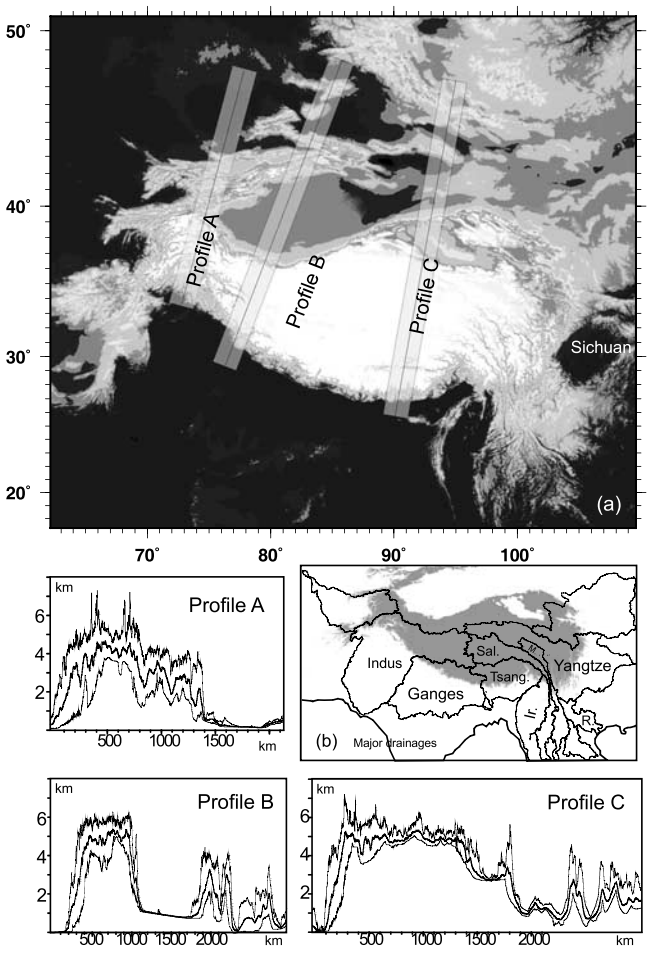

Figure 1. (a) Topographic image of the India-Asia collision zone showing the principal topographic divides and major drainages of the orogen (Mercator projection WGS84). (b) Major catchments around the India-Asia collision zone. Calculated with a 1′ (∼1.8 km) resolution digital elevation model using the software "River Tools." Sal., Salween River; M., Mekong River; Tsang., Tsangpo-Brahmaputra drainage; Ir., Irrawaddy River; R., Red River. The Marsyandi, Trisuli, Arun, and Sutlej rivers mentioned in text are all south draining contributories to the Ganges. Profiles A, B, and C are topographic swath profiles as indicated in Figure 1a. The different lines on each swath are as follows: The central line shows mean elevation of swath width; outlines show minimum and maximum elevation.

Plateau [e.g., *Burchfiel et al.*, 1995]. There is currently substantial debate if and when the Tibetan Plateau came to its present elevation, but many authors suggest that the uplift occurred no earlier than the late Miocene [*Spicer et al.*, 2003; *Clark et al.*, 2005a] and may be related to outward flow of material in the lower crust [*Clark and Royden*, 2000; *Beaumont et al.*, 2001; *Shapiro et al.*, 2004]. As such, it may postdate much of the deformation (and earlier continuous uplift) that accommodated the convergence since the initial collision around 50 Ma ago. Geometry and timing of this young uplift are as yet unknown, but it has been suggested that the uplift propagated eastward [*Schoenbohm et al.*, 2006b], raising an old relict landscape in eastern Tibet [*Clark et al.*, 2006] and "piling up" behind rheologically hard blocks like the Sichuan Basin, causing steep topographic gradients (Figure 1) [*Clark et al.*, 2005b]. Late uplift in the Tibetan Plateau, and also in the Himalayan range, is intimately related to the development of the major drainages around the orogen [*Brookfield*, 1998].

[5] Along the eastern margin of the Tibetan Plateau, the major rivers draining the plateau to the east and south are interpreted to have commenced an accelerated incision of an old relict landscape around 13 Ma [*Clark et al.*, 2005a]. The rivers Irrawaddy, Salween, Mekong and Yangtze flow parallel for much over 1,000 km and *Hallet and Molnar* [2001] have shown that these rivers can be used as markers for the finite strain in the region over much of the Miocene. However, the rivers flow in steep gorges which only formed after about 13 Ma preserving a much older landscape between them. This accelerated incision may be used as a proxy for the young uplift as it is likely to have occurred by rapid headward migration of knick points formed by relative base level lowering (i.e., plateau uplift) at the propagating topographic front. Thus, timing of increased incision rates and river piracy events can be used to infer the topographic evolution of the region. Most important of the piracy events is the capture of the Red River by the Middle Yangtze. This capture occurred in the mid-Miocene by headward migration of the Lower Yangtze from the Sichuan Basin in response to a young uplift event [*Clark et al.*, 2004]. This uplift is successively being documented by low-temperature geochronology [*Enkelmann et al.*, 2006] and landscape evolution studies [*Clark et al.*, 2006].

[6] In the syntaxes, both the Indus and the Tsangpo-Brahmaputra have a geometry that appears to be diverted by the collision process itself (Figure 1): they originate from the region northwest of Mt. Everest in the center of the orogen (but north of the Himalayan chain), flowing orogen parallel toward the syntaxes where they turn southward to traverse the syntaxes before ultimately draining into the Indian foreland. In the syntaxes, the Indus (in the west) and the Tsangpo-Brahmaputra (in the east) flow through the region of highest crustal thickening by the indentation. In these regions, they are responsible for the highest amounts of exhumation [*Treloar et al.*, 2003; *Massonne and O'Brien*, 2003]. In the eastern syntaxis it has been argued that the thickening itself is actually partly driven by the erosion of the Tsangpo-Brahmaputra drainage. *Zeitler et al.* [2001] argue that the massive erosion of this drainage is in fact responsible for enough exhumation and associated heat advection so that deformation is accelerated in this region and a stationary knick point is maintained by localized continuous uplift.

[7] Along the southern front of the orogen, drainages appear quite inconsiderate of the highest mountain range in the world: most rivers draining south flow right across the Himalayan range (Figure 1) [e.g., *Oberlander*, 1985]. This includes in particular the drainages contributing to the

Ganges including rivers like the Marsyandi or the Arun, or the Sutlej draining into the Indus. As such, the drainage divide is not located in the Himalayan range (where most of the tectonics occurs) but is displaced some 500 km toward the north (Figure 1b) [*Seeber and Gornitz*, 1983; *Bookhagen and Burbank*, 2006]. The origin of this counter intuitive geometry may be due to antecedent origin of the rivers, meaning that the age of the drainage is older than the age of the topography. In fact, the uplift of the Himalayan range has been attributed to the incision of these rivers itself [*Montgomery*, 1994] and is undoubtedly even younger than the Miocene uplift of the Tibetan Plateau [*Bookhagen et al.*, 2005; *Thiede et al.*, 2005]. Other interpretations of the crosscutting nature of the drainages in the Himalaya suggest that steep drainages along the Himalayan front migrated headward incising into the Plateau until they captured orogen parallel drainages along the northern margin of the chain. Our results presented below shed some light on the origin of this geometry and are alluded to in more detail by *Robl et al.* [2008].

[8] In summary, the drainages in and around the India-Asia collision zone show a close and partly counterintuitive relationship with the deformation and uplift in the region. Thus, the morphological record of these drainages is useful to extract information on the tectonic evolution of the orogen and ultimately on the feedback mechanisms between tectonic processes at depth and climatic and erosive processes at the surface. In the following we will use our numerical model to explore these relationships.

3. The Model

[9] In our approach we have coupled a mechanical thin sheet model designed to describe continental indentation and crustal thickening, with a landscape evolution model that describes erosion and crustal thinning. Additionally, we have inserted an independent uplift function: at specifically chosen time steps of the model runs we have synthetically uplifted the surface topography created by the mechanical model. We added this uplift in various geometries and time steps until the modeled geometry of the major drainages matches the observed geometry of the major Asian rivers. Through this, we aim to constrain the geometry of a late uplift observed in the region. Because of both, the erosion model and the independent uplift function, our model abandons the constant volume constraint of the classic thin sheet model.

[10] The mechanical model is that originally used to describe the India-Asia collision by *Houseman and England* [1986]. The model is a two-dimensional mechanical model in which the thin sheet approximation and a nonlinear viscous rheology are assumed. The model is implemented via a finite element code that has been expanded to a spherical geometry by G. A. Houseman (personal communication, 2005) and first used by *Robl and Stüwe* [2005]. In brief summary, the thin sheet model assumes that shear traction along the base of the lithosphere and the Earths surface are negligible and that, therefore, no vertical strain rate gradients need to be considered [*England and McKenzie*, 1982]. Then, the equations of force balance may be written in dimensionless form as

$$\frac{\partial \tau_{ij}}{\partial x_j} - \frac{\partial \tau_{zz}}{\partial x_i} = \frac{Ar}{2}\frac{\partial S^2}{\partial x_i}, \tag{1}$$

where S is the crustal thickness and τ_{zz} is the vertical principal deviatoric stress [*England and McKenzie*, 1982]. The subscripts i and j denote the two horizontal dimensions and the Einstein summation rule applies to double indices. The right-hand side of equation (1) is a term opposing crustal thickening because of buoyancy forces. In the formulation of equation (1) this is proportional to the Argand number Ar. The Argand number may be physically interpreted as the ratio of vertical to horizontal stresses and is explained in more detail by *England and McKenzie* [1982], *Robl and Stüwe* [2005], *Stüwe* [2007], and others. The forces described by equation (1) relate to strain rate in a nonlinear viscous constitutive relationship described by

$$\tau_{ij} = B\dot{E}^{\left(\frac{1}{n}-1\right)}\dot{\varepsilon}_{ij}. \tag{2}$$

In this power law rheology, τ_{ij} and $\dot{\varepsilon}_{ij}$ are the components of the two-dimensional deviatoric stress and strain rate tensor, respectively, where the subscripts refer only to the two horizontal coordinates as above. $\dot{E}$ is the second invariant of the strain rate tensor and n is a power law exponent. The proportionality constant B incorporates all material and temperature-dependent terms. It is equivalent to 2 times the viscosity ($B = 2\eta$) and has the units of [Pa s] if $n = 1$; that is, the viscous flow is Newtonian. However, for n ? 1, B is only a preexponent constant. Then, the viscosity is strain rate dependent, and only an effective viscosity can be defined from equation (1) from the ratio of stress and strain rate (for details, see, for example, the work of *Tenczer et al.* [2001]). Strain rate is defined in terms of the velocity gradients:

$$\dot{\varepsilon}_{ij} = \frac{1}{2}\left(\frac{\partial u_i}{\partial x_j} + \frac{\partial u_j}{\partial x_i}\right), \tag{3}$$

where u is velocity and i and j refer to the horizontal dimensions as above. Using this set of equations, nondimensional crustal thicknesses may be calculated as a function of time, using appropriate velocity or stress boundary conditions at the model margins. Elevation H and crustal thickness S is then dimensionalized using the reference values Ho = 100 m and So = 35 km. Surface elevations H during the subsequent evolutions are assumed to be supported by local isostasy so that they are proportional to crustal thickness:

$$(H - H_0)\left(\frac{\rho_m}{(\rho_m - \rho_c)}\right) = S - S_0. \tag{4}$$

The density contrast in equation (4) was chosen so that doubling the crustal thickness results in a surface elevation

of 4600 m, that is, with mantle density $\rho_m = 3100$ kg m^{-3} and crustal density $\rho_c = 2700$ kg m^{-3}.

3.1. Erosion Model

[11] The landscape evolution model used here is based on an empirical relationship between channel length and drainage area found by *Hack* [1957]. It is implemented via an erosion model for detachment limited transport that is applied to every grid node of the same triangulated finite element grid also used for the modeling of the mechanically driven deformation. For this erosion model it is assumed that the erosion-driven lowering of the topography occurs at a rate that is proportional to the area of the upstream drainage basin A as a proxy for water flux in the river (being, in turn, proportional to the basal shear stress exerted by the water onto its bedrock), and proportional to the square of the topographic gradient with distance L along a river channel dH/dL. This may be written as

$$erosionrate = -\frac{dH}{dt} = E \times A \times \left(\frac{dH}{dL}\right)^2, \quad (5)$$

where E is a proportionality constant of the units of m^{-1}s^{-1} (and is not to be mistaken for the quite different $\dot{E}$ in equation (2)). For our orogen-scale modeling we initially assume that E is a constant over the extent of the model region and discuss the implications of this assumption below. This model is closely related to the more classic stream power approach to erosion rate where stream power is typically defined as a general power law function of basin area (again being a proxy for water flux and thus basal shear stress) and linearly related to slope; that is,

$$\text{stream power} = s = A^{\theta}(dH/dL). \quad (6)$$

In this more common approach, the exponent θ is derived from logarithmic plots of channel length against basin area and is usually determined to be around $\theta = 3/7$ or $\theta = 0.5$ [*Wobus et al.*, 2006]. For equilibrium channels, the right-hand side of equation (5) corresponds to the classic definition of stream power with $\theta = 0.5$ as, in morphological equilibrium, the exponent may either be written as θ to A or as $1/\theta$ to slope. Here we also use $\theta = 0.5$ so that stream power has the units of meters.

[12] However, for channels not in equilibrium, it is not trivial if slope or water flux has a larger nonlinear contribution to erosion rate. In the absence of conclusive information on these contributions, *Wobus et al.* [2006] assumed that erosion rate is linearly proportional to stream power. This approach has the advantage that the proportionality constant has the units of reciprocal seconds and can be directly interpreted as a decay constant of topography. *Whipple and Tucker* [1999] present a discussion of the stream power approach and discussed the consequences of various assumptions on the nonlinear contributions of basin area and slope on the time-dependent evolution of river channels and on the evolution of disturbances like knick points. As there is not enough time-dependent information on the evolution of real river channels to resolve this discussion and as there is large discrepancies between engineering and geological communities on the exponents to A and (dH/dL), we follow here *Hergarten* [2002] and assume equation (5). Thus, the erosion rate is assumed here to be proportional to the square of stream power:

$$erosionrate \propto (streampower)^2. \quad (7)$$

We have also explored our model for exponents 1 and 2 and there is no general difference to the results. In fact, *Hergarten et al.* [2006] showed that equation (7) is a good approximation for erosion processes in general. Assuming A to control the water flux implies that there are no significant precipitation gradients across the model region and that, therefore, the surface runoff relates to the size of the upstream catchment area. This provides a simple model for the description of first-order features of drainage network development. The influence of precipitation gradients will be explored in the discussion section. In summary, the entire erosion process is driven by long-range transport according to equation (5) and no local mass balance (i.e., no diffusive slope processes) is considered. In other words, no sediment transport processes are considered and it is assumed that all material eroded at each point is lost through the model boundaries.

[13] Our model has the advantage that all erosional field variables are described by a single variable: E. A parameter value of $E = 1$ km^{-1} Ma^{-1} implies an erosion rate of 0.1 mm a^{-1} for a drainage basin of $A = 10^5$ km^2 size and a topographic gradient of $dH/dL = 0.001$. Erosion is driven by topographic gradients created by the mechanical thickening as described by equations (1)–(4). Compared to the original formulation, the implementation of the erosion model was transferred to a triangulated lattice of the mechanical model. We also added a simple model for deposition in closed basins. Finally, when horizontal extension leads to subsidence below sea level, such basins are filled to the default elevation H_0.

3.2. Model Geometry, Boundary Conditions, Parameter Values, and Grid Resolution

[14] The geometry and boundary conditions of the model we use here are identical to those used by *Houseman and England* [1986, 1993] for the original mechanical models to describe the India-Asia collision zone. These earlier models have successfully described a number of the first-order features of the Himalayan orogen [*Houseman and England*, 1996; *England and Houseman*, 1986; *Neil and Houseman*, 1997], and our results presented here can therefore be directly compared to the results of these earlier studies that did not consider erosion.

[15] The velocity field and other boundary conditions involve, among others, zero normal and tangential velocity at the northern and western boundaries, a lithostatic boundary (as defined by *Houseman and England* [1993]) in the east and a 25° inclined southern boundary. A 2,500 km long part of the southern boundary is assumed to have a curved shape to mimic the shape of the Himalayan arc (even at the

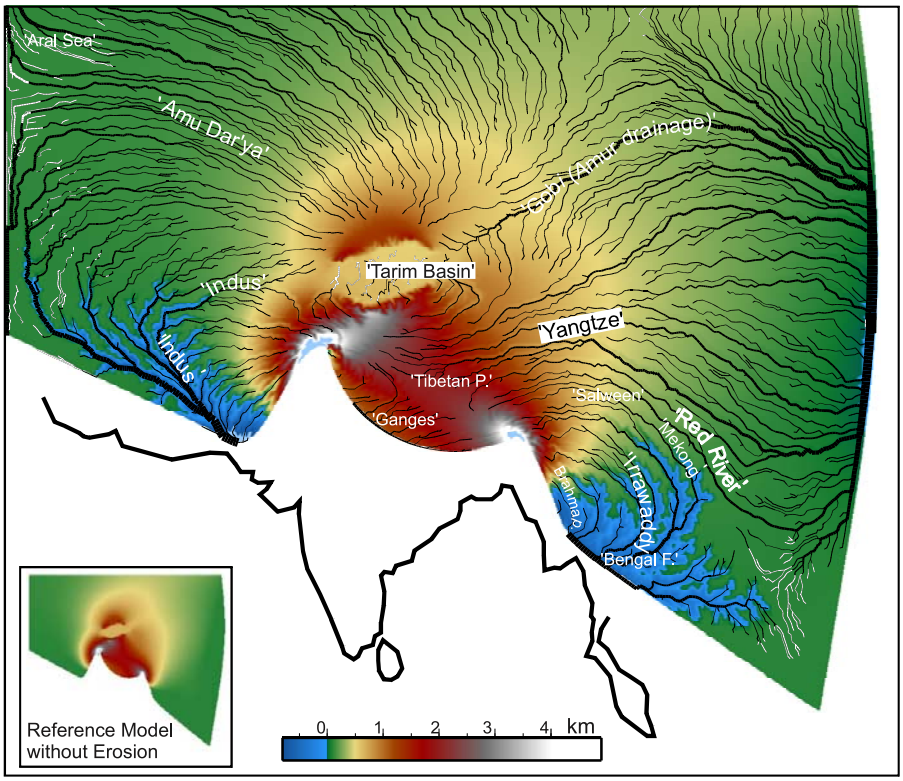

Figure 2. Interpreted model output of drainage development in the India-Asia collision zone for $n = 3$, $Ar = 1$. Drainages and topography (colored) are modeled from an initially flat region subject to the boundary conditions described in the text, and their shape is entirely dynamically formed during the model run. The shown result is after 50 Ma of convergence at a rate of 5 cm a^{-1}. Asia outline and labels on rivers are interpreted and only superimposed for the discussion. Black parts of drainages indicate erosion; white parts are areas of deposition. The inset shows the reference model without erosion and is identical to that used by *Houseman and England* [1996].

start of the runs) and is moved northward at a constant rate of 5 cm a^{-1}. The dimensions of the model region are scaled to a length of 10,000 km width and an initial elevation of 100 m. The only further concession we make on approximating the geometry of the India-Asia collision zone is by placing an irregular hexagonal region in the approximate position of the Tarim Basin that remains rigid [e.g., *Neil and Houseman*, 1997]. We assume that this region is $100^{1/n}$ times as viscous (see equation (2)) as the remainder of the model region. Aside from the Tarim Basin, the Sichuan Basin also formed a rigid block to the north and east of the Tibetan Plateau, but we do not consider this initially. Its influence on the evolving drainage geometry is explicitly discussed in later sections of this paper.

[16] Initially (for Figure 2), we assume only one set of assumptions for the mechanical parameters of the modeling, namely those that *Houseman and England* [1996] derived as their best fit parameter for the India-Asia collision zone. We assume a power law exponent in equation (2) of $n = 3$ and an Argand number in equation (1) of $Ar = 1$. We note that higher power law exponents cause a more spatially confined Tibetan Plateau with steeper topographic gradients on its side and we shall explore the consequences of this for the landscape development further below. It is also noted that Ar (as well as E, n and other parameters) may vary spatially over the extent of the model region. However, it is the defined aim of this study to keep the assumptions as simple as possible and we therefore follow earlier studies and assume that Ar is constant over the extent of the model region.

[17] For Figure 2 we also assumed an erosion parameter of $E = 4$ km^{-1} Ma^{-1}. Only results after 2,500 km of convergence (i.e., after 50 Ma) are shown and internal deposition is allowed in closed basins. In comparison to the India-Asia collision zone this is probably realistic as the size of the model region encompasses substantial parts of the Indian Ocean, where the Bengal Fan accommodates much of the material eroded from the orogen. Later (Figures 3 and 10) we then explore the results of varying the erosion parameter E and consider precipitation gradients in the formulation of equation (5).

[18] The numerical discretization of the erosion model of equation (5) causes an overestimate of the erosion rate in areas where drainages are parallel for coarse triangulations: Then basin areas of parallel rivers will be overestimated causing a synthetic focusing of the surface run off, resulting

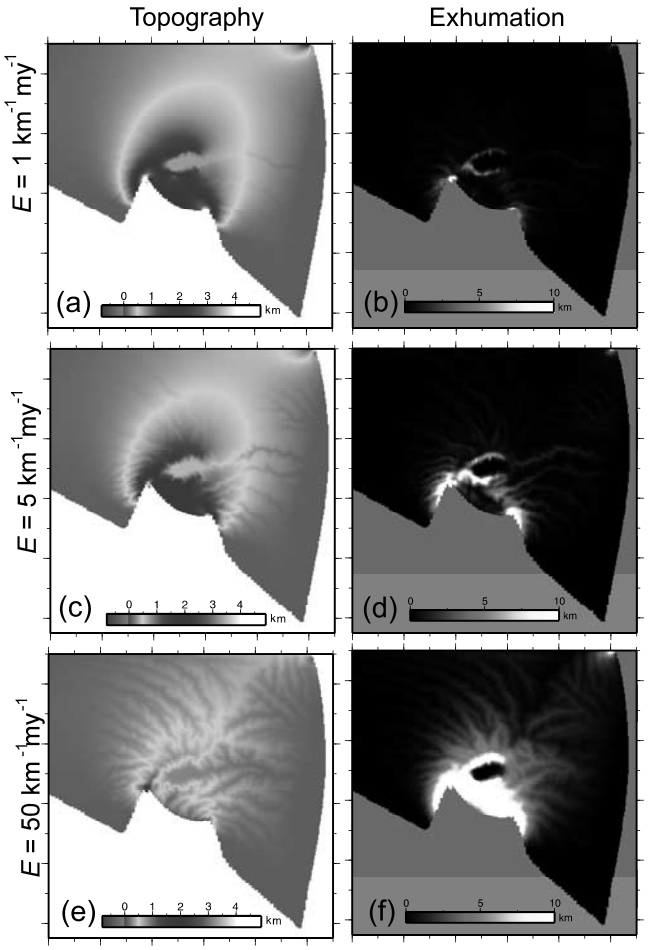

Figure 3. (a–f) Topography and exhumation in the modeled collision zone after 50 Ma of convergence for three different erosion parameters. Power law exponent in the stress-strain rate relationship is $n = 3$, and the Argand number is $Ar = 1$. Note that the distribution of exhumation does not always correspond to the distribution of elevation. For example, exceptionally high exhumation occurs at the north margin of the Tibetan Plateau, although the surface elevation is not as high as in the syntaxes or in the Himalaya.

in an overestimate of the erosion rate. This effect does not occur when drainage patterns are dendritic, but there are several regions in the India-Asia collision zone where this can affect the results: Near the indenter front the steep topographic gradients cause rivers to be parallel, as observed in the Himalaya where the rivers crossing the range are more or less parallel (Marsyandi, Dudh Kosi, etc. [see *Robl et al.*, 2008]). Similarly, near the eastern syntaxis, four of the largest rivers in Asia are near parallel (Irrawaddy, Mekong, Salween, and Yangtze). In order to circumvent this problem we have chosen a model resolution that is comparable to the mean distance of major rivers crossing the Himalaya (triangle area = 20,000 km^2). It also should be noted that, because we assume local isostasy, river incision will be compensated by isostatic rebound on a node by node basis so that the modeled topographic expression of deeply incising model rivers remains smaller than it would in nature. Because of the dependence of the results on grid resolution and the assumption of local isostasy, some of the capture events discussed below occur slightly earlier or later, depending on the grid resolution. Nevertheless, large numbers of numerical experiments with a series of grid resolutions showed that the fundamental conclusions drawn below are robust toward the number of mesh nodes.

4. Results

[19] We begin by showing a model result using the default parameters discussed above (Figure 2). For illustration purposes we also have not synthetically filled areas were subsidence occurs below sea level and allow erosion/sedimentation in these regions when closed basins occur (sedimentation in white parts of drainages on Figure 2). Figure 2 shows that drainages develop, expectedly, radially around the indenter front, following the topographic gradients. It may be seen that the developing first-order drainage geometry has some similarities with those observed in the India-Asia collision zone. Although the erosion model causes substantial exhumation of rocks in parts of the model region where topographic gradients are steep (Figure 3), there is no fundamental difference between the modeled topography and the topography when ignoring erosion (inset in Figure 2). Several important features of the evolving drainage pattern may be seen in Figure 2.

[20] First, and importantly to the interpretation of the India-Asia collision zone, a narrow zone north of the indenter front (labeled "Ganges") develops that drains southward (in all further discussion geographic locations referred to in quotes are those interpreted from the models; without quotes they refer to real geographic features in nature). This corresponds to the position of the drainage divide in the India-Asia collision zone and provides a considerable improvement over earlier model that did not consider erosion. The southward draining zone terminates at the syntaxes of the indenter and widens to its center. The maximum width of this zone is about 10% to 20% of the width of the indenter (250–500 km when scaled to a 2,500 km wide indenter). This zone is partly caused by the curvature of the indenter, but mostly depends on the topographic gradient across the indenter front. It has a small variation for large variations in erosion rate (see below). Near the corners of the indenter, developing drainages adapt concentric patterns.

[21] Sedimentation occurs in the "Tarim Basin" and in the northwestern part of the model region ("Aral Sea"). In contrast, no sedimentation occurs in the "Yangtze," "Red River," "Salween," and "Mekong" rivers (except in those parts that are below sea level; see model assumptions above) because the open eastern boundary allows lateral extrusion. Highest topography is developed in the syntaxes where drainage basins (and therefore stream power) are too small to affect topography in a significant way (although we shall show later that exhumation in these regions is significant). Rapid extension behind the indenter (e.g., southeast

of the eastern syntaxis) causes a strictly parallel orientation of the developing drainage pattern, as is observed in the course of the Irrawaddy, Mekong, Salween, and Red Rivers (Figure 1).

[22] Figure 3 shows only the final time steps of three different model runs with different erosion parameters. Earlier time steps show that the drainage patterns are initiated in their final geometry very early on in the model evolution and no major capture events occur during the subsequent time-dependent evolution. Drainage patterns change mostly by horizontal strain and advection of existing valleys. *Hallet and Molnar* [2001] suggested that the curvilinear drainages in the three rivers region (Salween, Mekong, and Yangtze region) can be interpreted as passive strain markers, and the result of Figure 2 confirms this interpretation. The fact that major capture events on all scales have been documented in the collision zone [e.g., *Clark et al.*, 2004], in particular along the east margin of the Plateau, is likely to be related to other causes discussed below.

4.1. Thinning Versus Thickening

[23] The erosion parameter assumed in Figure 2 (E = 4 km^{-1} Ma^{-1}) is large enough to cause all the features of the drainage development described above, yet small enough to retain a high elevation with little exhumation in the Tibetan Plateau. In order to explore the effect of varying E and constraining a best fit mean erosion parameter for the entire model orogen, Figure 3 shows the model topography for E = 1, 5 and 50 km^{-1} Ma^{-1}. For E = 1 km^{-1} Ma^{-1}, little change in the topography occurs compared to models without erosion (Figure 2, inset, and Figure 3a). Crustal thickness and surface elevation correspond largely to those predicted by *Houseman and England* [1996], and erosion does not cause valley incision that would be large enough to be noticeable in the color shading (approximately 500 m relief). In contrast, for E = 50 km^{-1} Ma^{-1} (Figure 3e) the topography is largely destroyed by erosion. The ''Tibetan Plateau'' is completely dissected by drainages and the only place of some significant topography remains near the western syntaxis of the Himalaya. An intermediate erosion parameter around E = 5 km^{-1} Ma^{-1} reproduces many of the features observed for the orogen (Figure 3c): The ''Tibetan Plateau'' is retained north of the indenter front, it is flat with steep gradients on its sides, the absurdly high topography produced in the syntaxes in Figure 3a is rapidly eroded, and drainage incision causes significant valley erosion resulting in valleys that can be noticed on the resolution of Figure 3c. We conclude that an erosion parameter for the India-Asia collision around E = 4–5 km^{-1} Ma^{-1} is reasonably well constrained. A value of E = 5 km^{-1} Ma^{-1} corresponds to a mean erosion rate of 0.5 mm a^{-1} for rivers with a channel gradient around dH/dL = 1‰ and a drainage basin of A = 10^5 km^2 size. This value for erosion rate has actually been documented for the eastern Tibetan Plateau by *Clark et al.* [2005a] using geochronologically derived incision rates.

[24] This qualitative fit of the topography for E = 5 km^{-1} Ma^{-1} is also confirmed by the amounts of exhumation for n = 3 as used here. Figures 3b, 3d, and 3f illustrate the time-integrated effects of erosion at every grid node. Interestingly, the spatial distribution of exhumation does not exclusively correspond to the regions of high topography or even to that of the high topographic gradients because horizontal advection of regions of high stream power causes lateral shifts in the points of maximum elevation and erosion from the regions of maximum time-integrated erosion (i.e., exhumation). Independently of the erosion parameter, the exhumation is always a maximum in the ''syntaxes,'' a minimum in the ''Tarim Basin'' and reasonably high at the margins of the ''Tarim Basin'' where the topographic gradients are high. However, whether or not erosion affects the ''Tibetan Plateau'' enough to cause exhumation of rocks from midcrustal levels (i.e., many kilometers) depends strongly on the erosion parameter. For an erosion parameter around 5 km^{-1} Ma^{-1}, the ''Tibetan Plateau'' remains practically unaffected in both its topography and its exhumation, while there is significant exhumation of rocks from midcrustal levels and more in the syntaxes, in the ''Kun Lun'' region and in the ''Tien Shan.'' This corresponds well to observations by metamorphic geologists reporting of high-grade metamorphic parageneses from some of these regions [e.g., *Massonne and O'Brien*, 2003; *Treloar et al.*, 2003]. The exhumation of the Central Himalayan Crystalline Complex between the Main Central Thrust and the South Tibetan Detachment Zone at the southward facing slope of the Himalaya is not predicted by our model. However, the exhumation of this complex is caused by wedge extrusion [*Vannay et al.*, 2004], channel flow [*Beaumont et al.*, 2001], or other processes that must be studied in cross section. At erosion parameters below E = 5 km^{-1} Ma^{-1} no significant exhumation occurs anywhere outside very small regions around the syntaxes (Figure 3b). Conversely, for E = 50 km^{-1} Ma^{-1} or higher the entire model orogen experiences significant exhumation including the region of the ''Tibetan Plateau'' where, in reality, negligible exhumation occurred in recent times. As such, this erosion parameter is clearly too high (Figure 3f). Again, it may be concluded that E = 5 km^{-1} Ma^{-1} provides a reasonable mean estimate for the erosion parameter (Figure 3d). Interestingly, the prediction for exhumation (and elevation) for an erosion parameter of E = 5 km^{-1} Ma^{-1} reproduces observations from large regions of the India-Asia collision zone, despite strong precipitation gradients observed across the orogen.

[25] The general results of Figure 3 can be quantified better by investigating profiles through the model region. The three profiles shown in Figure 4 are chosen so that they cross the western syntaxis by passing the ''Tarim Basin'' (profile A), cross the center of the range (also crossing the ''Tarim Basin''; profile B), and go through the eastern end of the range in the region of Mt. Everest bypassing the ''Tarim Basin'' through the ''Qiadam Basin'' (profile C), respectively. The first and probably most significant finding of Figure 4 is that the north-south profiles across the orogen appear to be qualitatively consistent with the observed topography (Figure 1): The westernmost profile (Figure 4, profile A, solid line) rises abruptly from the south and then drops continuously toward the north into central Asia; the

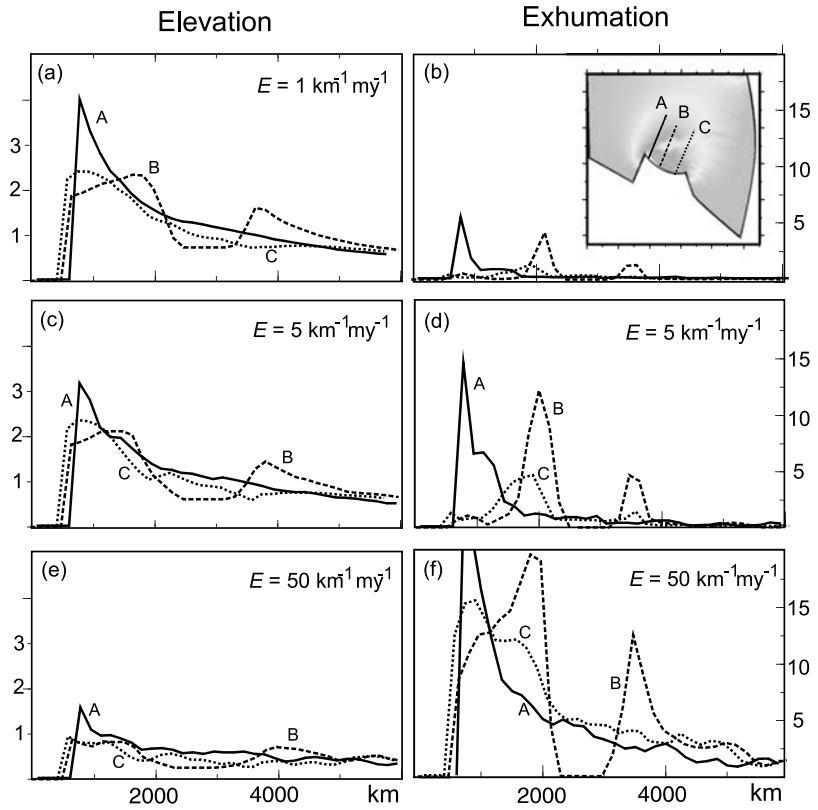

Figure 4. (a–f) Topography and exhumation along three different profiles across the model region as shown in the inset. Note that for the best fit erosion parameter from Figure 3, the maximum elevation is merely of the order of 2–3 km. Compare with Figure 1 for true topographic profiles through the orogen.

central profile (Figure 4, profile B, dashed line) rises onto the "Tibetan Plateau," and then drops abruptly into the "Tarim Basin" before rising to a secondary peak in the "Tien Shan." The third profile (Figure 4, profile C, dotted line) crosses the Everest region and passes east of the Tarim Basin into central Asia and the modeled elevation changes correspond to this.

[26] In contrast to the qualitative fit of the profiles, the quantitative values for the modeled elevations are inconsistent with the observed surface elevations in Tibet (compare Figures 1 and 4): In general, modeled elevations are about 2–3 km lower than the observed absolute elevations in the Himalaya and the Tibetan Plateau. This result has already been obtained by Houseman in the original papers where a maximum crustal thickness of around 60 km was only attained in the syntaxes, but it becomes much better constrained here as we have demonstrated that erosion for the best fit erosion parameter only thins the crust by some few kilometers in both model and nature. Crustal thickness and modeled elevations are therefore in contrast to the observed surface elevation and an observed thickening up to 80 km (as recorded by, for example, the INDEPTH project [*Nelson et al.*, 1996]) and confirm the need for an alternative interpretation. Aside from invoking late uplift through mantle processes or thickening of the crust only [*Royden*, 1996], a more extreme nonlinearity in the stress-strain rate relationship may also provide an explanation for higher crustal thickness underneath the Tibetan Plateau. This idea is supported by the high topographic gradients at the Plateau margins.

4.2. Steep Topographic Gradients of the Tibetan Plateau

[27] One of the puzzling features related to the India-Asia collision zone is the steep topographic gradients at the northern edge of the Tibetan Plateau. Figure 1 shows that these are in fact substantially steeper than predicted by the model runs shown in Figures 2 and 3. Clearly this also has an influence on the drainage development and needs consideration. Several reasons may be responsible: First, it may be due to rheological differences between the crust in the Tibetan Plateau and the central Asian foreland. The model of *Clark et al.* [2005b] suggests that the steep gradients were built up owing to "piling up" of material behind rheologically hard blocks in Asia, like the Sichuan Basin. *Neil and Houseman* [1997] already suggested on the basis of mechanical modeling that the Tarim Basin is best described as a hard block. However, the steep topographic gradients may also be due to an extreme nonlinearity of the stress-strain rate relationships. A highly nonlinear relationships between

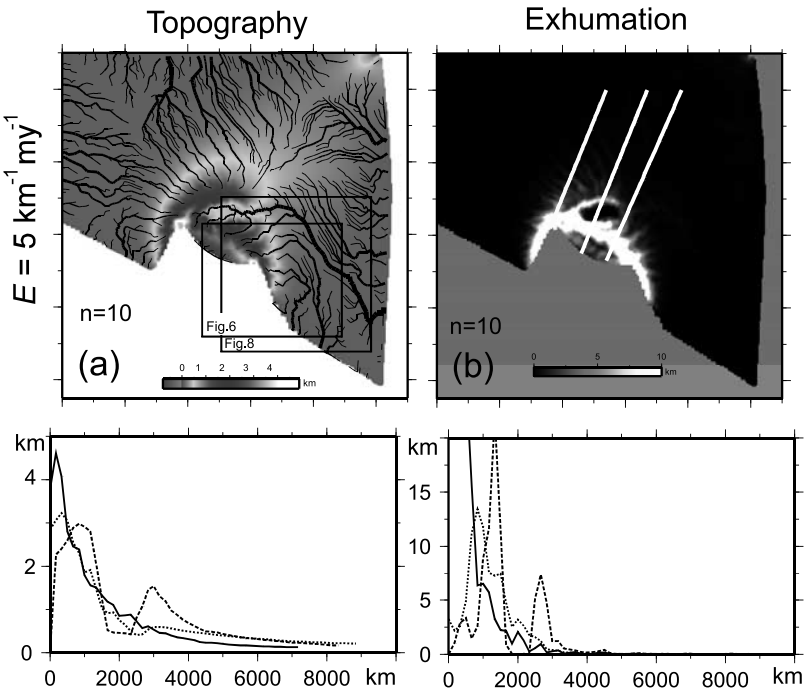

Figure 5. (a and b) Topography and amounts of exhumation in plan view and cross section as for Figures 3 and 4 but with a power law exponent of $n = 10$ and $Ar = 1$. Because of this extreme nonlinearity of the stress-strain rate relationship, elevation and topographic gradients at the north margin of the ''Tibetan Plateau'' and in the ''Tien Shan'' are substantially higher (and more similar to reality) than in Figures 2, 3, and 4. Nevertheless, the geometry of the major drainages appears largely independent of the power law exponent. Boxes show regions enlarged in Figures 6 and 8.

stress and strain rate (e.g., large n in equation (2)) causes focusing of deformation into smaller regions with steep strain gradients at the margins of the deforming region. In the model runs discussed above, we used a power law exponent of $n = 3$ as suggested by *England and Houseman* [1986] for the India-Asia collision zone. In order to explore for higher nonlinearities, a series of runs were performed with $n = 5$ and $n = 10$ (and $Ar = 1$). Figure 5 shows the results for $n = 10$. The topographic gradients at the north margin of the Plateau become significantly higher than in Figures 2 and 3 and are similar to those observed. Nevertheless, crustal thickness and surface elevation of the ''Tibetan Plateau'' do not increase significantly, confirming the need for an independent uplift that explains the high elevation. Moreover, the steep gradients also cause focusing of erosion and exhumation, and although the topography of the Tibetan Plateau is better predicted with $n = 10$ (Figure 5a) than with $n = 3$ (Figure 3c), the amount of exhumation is not: Figure 5b indicates that substantial portions of the northern ''Tibetan Plateau'' should experience massive exhumation for $n = 10$. Surface exposures of metamorphic rocks from midcrustal levels should occur in a band along the entire northern side of the Tibetan Plateau that joins both syntaxes. In contrast, the distribution of metamorphic rocks in the India-Asia collision zone corresponds much more to that seen in Figure 3d. We conclude that the steep gradients are unlikely to be related to extreme stress- strain rate relationships and are more likely to be caused by rheological contrasts as well as independent uplift. Thus, our model is in support of lower crustal flow models suggested by *Clark and Royden* [2000] (see also data by *Shapiro et al.* [2004]).

5. Discussion

[28] The results presented above show that many of the first-order morphological features of the India-Asia collision zone can be reproduced with a startlingly simple set of model assumptions. Although this is a nice reproduction of the natural setting, in some ways, this comes to no surprise: the model drainages develop radially outward from the zone of highest topography. Time-dependent model evolutions toward the final time steps shown in Figures 3–5 show that the drainage patterns develop in their final geometry very early on in the evolution of the runs and are subsequently not captured into dramatically different orientations. As such they may act as strain markers. This was in fact suggested by *Hallet and Molnar* [2001]. Conversely, observed capture events may be a record of a late independent uplift event as suggested for the eastern Tibetan Plateau. Thus, the differences between stream power in modeled versus actual rivers may provide

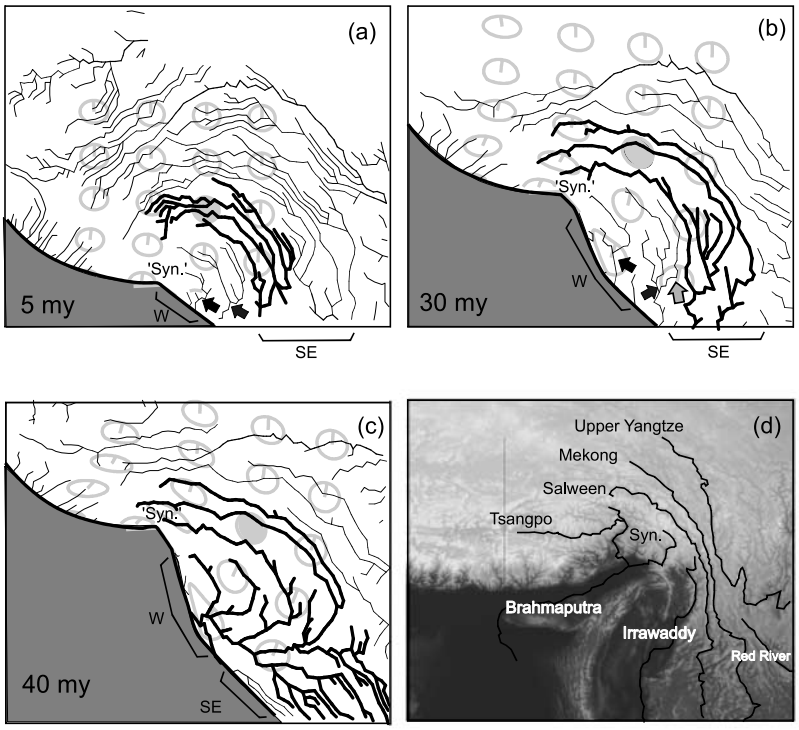

Figure 6. Time-dependent model evolution of part of the model region from Figure 5. Strain markers are superimposed. (Grey shaded strain marker is discussed in text.) (a–c) The model geometry 5, 30, and 40 Ma after onset of collision (at 50 Ma before present). (d) A topographic map of the eastern syntaxis with a few of the large rivers labeled. Note that the drainages are already initiated early on in a curvilinear fashion around the syntaxis. Labels "W," "SE," etc., and arrows are discussed in text.

limits on the geometry of the late uplift. Some of these points will now be investigated.

5.1. Competing Advection and Erosion in the Eastern Syntaxis

[29] In order to study the competition of strain, erosion, and capture around the eastern syntaxis, Figure 6 shows the time-dependent model evolution of a small area of our model. It is the same model for which the final time step was interpreted in Figure 5. Strain markers are superimposed for the interpretation and one drainage system is shown in thicker lines to ease the discrimination between different drainage regions in Figure 5. Although the geometry of the model run is extremely simplified from the natural geometry of the syntaxis, some features are similar to the orogen (shown in Figure 6d) and may aid the interpretation of its evolution. For our discussion, we interpret model drainages meeting the model boundary in Figure 6 at "W" as those that drain westward into the Brahmaputra River and those draining at "SE" as southeast draining rivers like the Salween, Mekong, or Red River. Then, the following aspects may be interpreted from Figure 6:

[30] 1. The curvilinear arrangement or the drainages is initiated very early on in the model runs (i.e., in Figure 6a). It is the consequence of the rivers flowing radially outward from the high topography in the syntaxis and being horizontally bent by the deformation. In the model, as in nature, the region of most rapid extension and dextral shear is in the trailing edge of the indenter southeast of the syntaxis. The curvilinear arrangement is retained through the entire evolution. However, the increasing distance between the indenter front and the model boundary at "SE" causes successive stretching of the rivers extending the arc of curvature throughout the evolution.

[31] 2. Changes in the proximity of parallel rivers over time occur owing to a competition between two factors: The first factor is deformation of the crust, which moves the drainages closer according to the finite strain. Comparing Figures 6a and 6c, a strain of about 2 has occurred owing to deformation (gray shaded strain marker) in the region of the thick drawn system. This deformation moved drainages closer to each other by a factor of about 2. The second factor is separating drainages by capture events that focus the surface runoff into major drainages and desert minor ones. In the model evolution shown in Figure 6, the minor capture events win over the strain, so that the distance between major valleys increases, rather than decreases, over time. This is consistent with the interpretation of *Clark et al.* [2006], who argue that much of the landscape preserved between the gorges of the major rivers reflects an old relict landscape.

[32] 3. Capture of drainages draining southeast by small drainage basins draining westward into the syntaxis occurs quite late in the model evolutions. In Figure 6b, the small

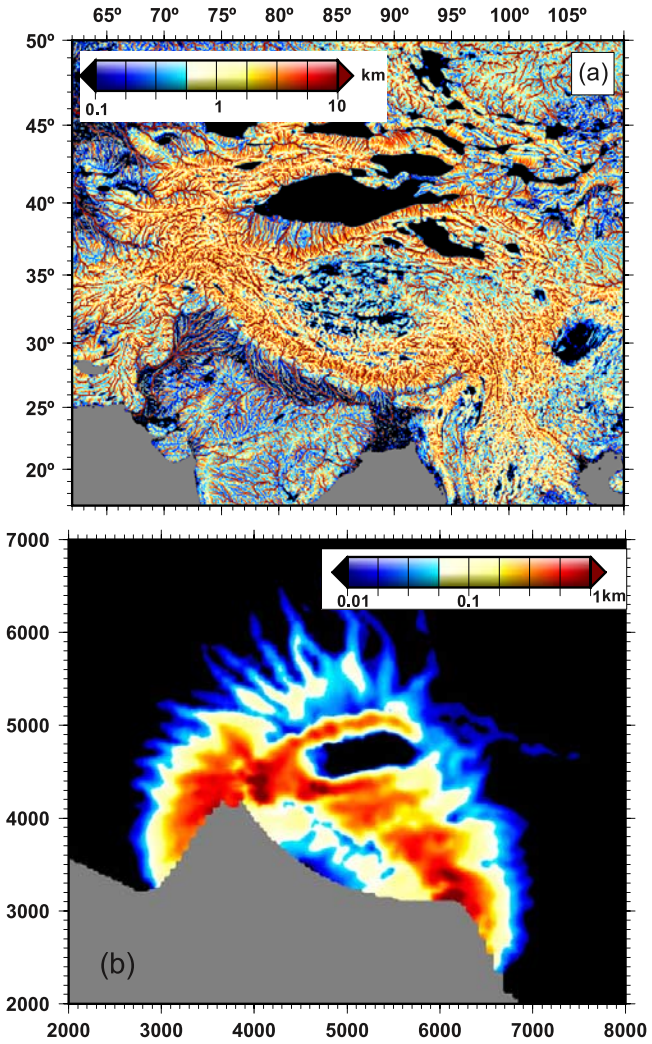

Figure 7. (a and b) Stream power in the India-Asia collision zone and in the model. See equation (6) for a definition of stream power measured here in kilometers. Color shading is logarithmic, and a 10 km wavelength filter was applied to the digital elevation model prior to calculations.

drainages labeled with the black arrows remain separate from the major drainages shown in the thick lines for most of the evolution. This is because the topography buildup in the syntaxis initially diverts drainages to flow outward from the syntaxis. However, the small drainages that do flow west get successively steepened up so that they cause headward cutting and eventually capture major drainages flowing southeast. In the model evolution this occurs between 30 and 40 Ma after the start of collision (between Figures 6b and 6c) at the point labeled with the gray arrow.

5.2. Degree of Geomorphic Equilibrium

[33] In the model runs no major river capture events occur. This may be due to three reasons: (1) The forward propagation of the region of highest deformation (and uplift) into the foreland shifts the formation of knick points more rapidly downriver than their upriver migration due to erosion. (2) Horizontal advection and extension of drainages by horizontal strain prevents the upward migration of knick points. (3) The best fit erosion parameter is large enough to maintain a quasi–steady state equilibrium of the drainages where excesses in stream power of the equilibrium value are balanced by the uplift rate. This third point can be tested by deriving stream power and comparing this to uplift rate in both model and nature.

[34] Figure 7 shows a comparison of the stream power calculated from a digital elevation model for the India-Asia collision zone (Figure 7a) with that of the model run also shown in Figure 5 ($Ar = 1$, $n = 10$; Figure 7b). Stream power varies between $s = 0.01$ km and $s = 10$ km in both model and orogen for most of the region, although in the model stream power appears lower, owing to the large flat part of the model region (black parts of Figure 7b). In the model (Figure 7b), stream power appears to relate to topography and forms a radial pattern. Although stream power appears to have a maximum on the "Tibetan Plateau," comparison with Figure 5 shows that it is highest where the topographic gradients (and not elevation) are the steepest. This is in a band joining the syntaxes north of the indenter. In contrast to nature (Figure 7a), stream power is low near the indenter front because drainage areas are small and topographic gradients at the indenter front are low. To a first-order approximation, elevation in the model runs shown here also correlates with uplift rate so that stream power roughly corresponds to uplift rate. This indicates that variations in stream power are caused by surface uplift: For a region with a constant spatial and temporal uplift rate, stream power should be a constant when the channels are in equilibrium. When stream power varies, but correlates closely with uplift rate, then a steady state is likely to be balanced where the stream power variations are compensated with uplift rate variations.

[35] In contrast, in the India-Asia collision zone, stream power forms a maximum in a ring shaped area around the Tibetan Plateau apparently related to the topographic gradients (Figure 7a). In the Pamirs and along the east margin of the Plateau (where surface elevations begin to decrease toward the Kasachstan Plane and the Sichuan Basin, respectively) stream power is a maximum, while it is extremely small on the Tibetan Plateau where topographic gradients are low. We interpret this distribution of stream power as an indication for late uplift with the ring shaped maximum roughly outlining the geometry of this uplift.

[36] In order to explore this in some more detail, we have investigated channel profiles of some major rivers draining across the edge of the plateau. Figure 8 shows a detail of the east margin of the Tibetan Plateau both as topographic map of the region (Figure 8a) and part of the model result from Figure 5 (Figure 8b). Channel profiles are calculated for two model rivers called the "Salween" and the "Yangtze" and two real rivers: the Salween and the Yangtze. In Figure 8e we have also plotted the Red River because the Red River formed probably the downstream extension of the Upper Yangtze prior to its capture [*Clark et al.*, 2004, 2005a]. It may be seen that the model channel profiles (Figures 8d and

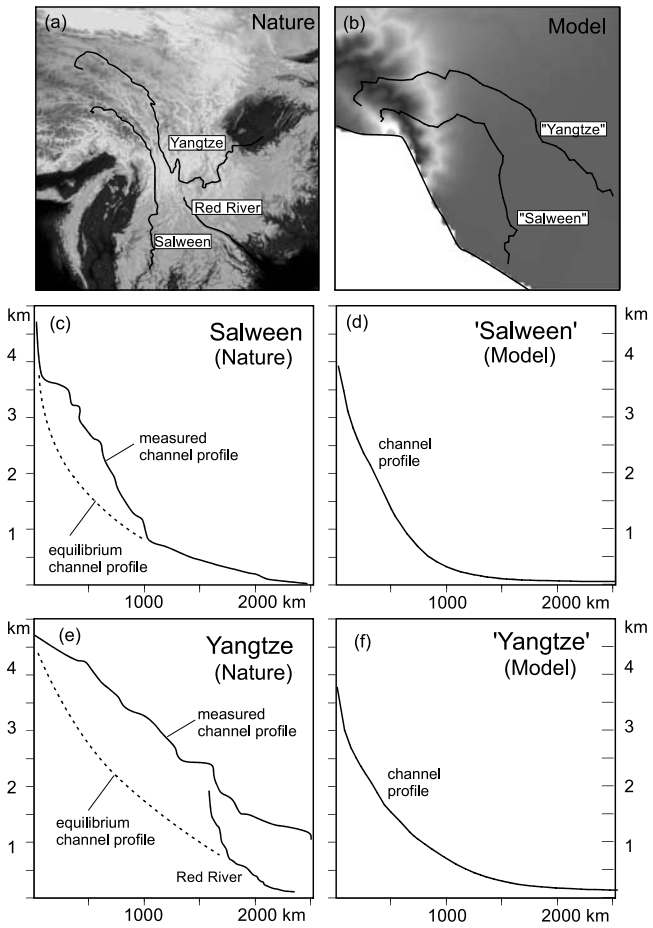

Figure 8. (a–f) Channel profiles for the Yangtze, Salween, and Red Rivers, as well as for model drainages that roughly correspond to the course of these rivers (here labeled "Salween" and "Yangtze").

8f) follow relatively smooth equilibrium patterns (constant color along channel). Small breaks in slope correspond to discontinuities in the area-distance relationships and therefore to jumps in stream power, but no massive knick points occur. In contrast, both the Yangtze–Red River system and the Salween River deviate massively from a concave channel profile in the upper 1,500 km and 1,000 km, respectively. Both of them have a 1,000 km long convex part of the channel profile in the eastern Tibetan Plateau where they drain through a region where the stream power has a maximum in Figure 7a. The dotted lines in Figures 8c and 8e indicate, qualitatively, the shape of the expected equilibrium channel profile. It is suggested that these convex portions of the channel profiles geographically relate to regions of late uplift.

5.3. Constraints on Late Uplift and Capture Events

[37] In summary, the results presented above constrain late uplift in the India-Asia collision zone from two pieces of evidence: First, Figures 2–5 show that the modeled crustal thickening is insufficient to reproduce the observed crustal thickness. This confirms results of earlier models for the India-Asia collision zone. Second, Figures 6–8 show that the geomorphic disequilibrium indicates that the geometry of surface uplift is inconsistent with that expected by indentation and that an independent uplift event must be invoked in the model to account for the morphological observations. Late surface uplift in the India-Asia collision zone is still very much debated. *Brookfield* [1998] recognized that the capture events of the major drainages may place some constraints on this uplift. *Clark et al.* [2005a] have suggested that this uplift must have a wavelength of at least 1,000 km but could not constrain which part of the surface topography is due to the late uplift beyond the fact that they suggest that it probably follows the east margin of the present-day plateau.

[38] Of the capture events in the collision zone, the most dramatic one is probably the capture of some of the curvilinear drainages flowing south around the eastern syntaxes by eastward draining rivers. In particular, this is the capture of the Upper Yangtze by the Lower Yangtze which now causes much of the Yangtze River to drain through the Sichuan Basin toward the east, leaving the Salween, Mekong and the relatively short Red River and its large delta as the remaining evidence of a major drainage system flowing south [e.g., *Clark et al.*, 2004]. Second, there is the capture of the Yarlong-Tsangpo by the Brahmaputra River to drain southwest through the syntaxis into the Ganges Plain. It is possible that the Yarlong-Tsangpo River once was part of a major southeast draining system of rivers that still includes the Salween and Mekong [*Clark et al.*, 2004]. Its capture by the Brahmaputra is thought to have been caused by headward migration of an over steepened course of the Brahmaputra into the syntaxis [*Clark et al.*, 2004; *Robl et al.*, 2008].

[39] In order to reproduce these capture events we have inserted an independent uplift function into the model runs shown in Figure 5 (Ar = 1, n = 10) at 35 Ma after initial collision (i.e., 15 Ma before present): At this time we have uplifted the surface elevation of part of the model region by variable amounts of 500–2,000 m distributed over a time period of 5 Ma (i.e., between 35 and 40 Ma). As a consequence of this external uplift, the model is not volume constant anymore. We use this synthetic raising of the topography as a model description for Miocene uplift processes in the Tibetan Plateau like crustal injection or delamination of the mantle part of the lithosphere. We experimented with a series of geometries for this late uplift (Figure 9). None of the outwardly convex uplift shapes was able to produce capture of the Yangtze River (i.e., uplift geometries 1, 2, and 3 in Figure 9a). This is because the margins of outwardly convex uplift functions are more or less normal to the drainages, enhancing existing topographic gradients but not diverting drainages. As a consequence, they cause local increase in stream power and minor capture events between parallel rivers, but no major eastward diversion in the central parts of the rivers.

[40] We have therefore experimented with an uplift region that has an outline with concavities around some of the blocks suggested in the literature to be rheologically

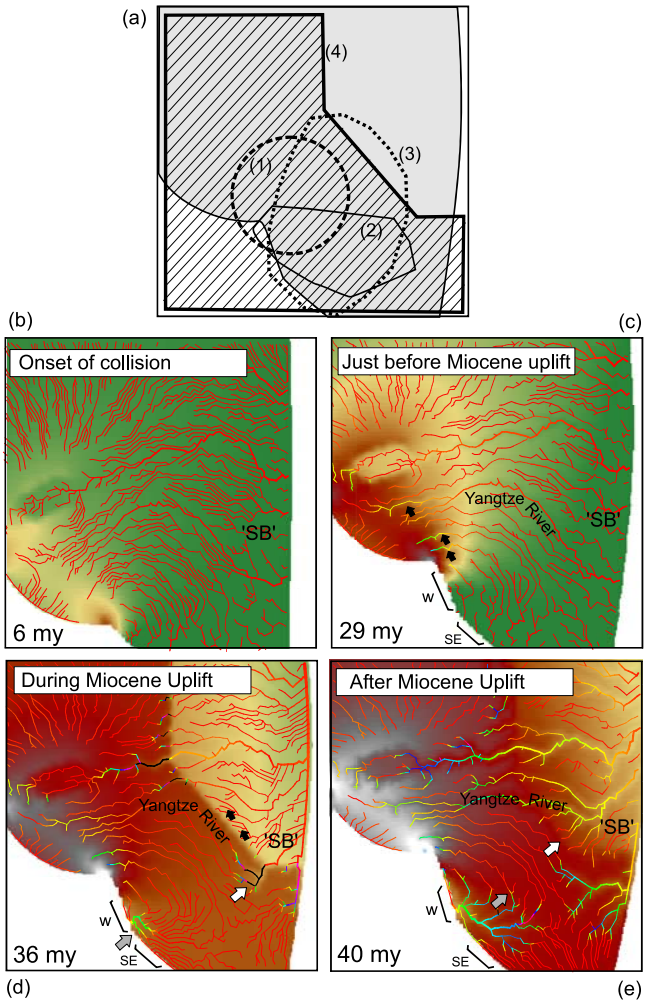

Figure 9. Geometrical constraints on the late uplift. Times are labeled in millions of years after initial collision (at 50 Ma). (a) Different uplift functions we experimented with. The shaded region shows the model region at 30 Ma after the start of the model run. The thick, thin, dotted, and dashed lines show the outlines of areas over which an independent uplift of 1,000 m was invoked at time 30 Ma. Uplift distribution (geometry 4, cross-hatched region) reproduced the capture of the Yangtze River. (b–e) Four time steps of a model run in which uplift distribution (geometry 4) was added in addition to the dynamically created surface uplift at 30 Ma after onset of deformation. Erosion parameter is $E = 5\ \mathrm{km}^{-1}\ \mathrm{Ma}^{-1}$. Color of the model region indicates topography in the same color scheme as that in Figures 3 and 5. Color of rivers indicates stream power. Black sections are where stream power exceeds the scale. SB, Sichuan Basin.

hard. Of these, the most simple uplift function uplifts the entire model region, except the region roughly where the "Sichuan Basin" is located (uplift distribution, geometry 4 in Figure 9a). An uplift function that uplifts the entire region outside the Sichuan Basin does indeed reproduce the major observed capture events for uplifts more than 500 m of uplift. An uplift of 1,000 m or more within the 5 Ma period between 35 and 40 Ma causes first capture of the Middle Yangtze and subsequent capture of the Upper Yangtze in the sequence interpreted by *Clark et al.* [2004] and in a very similar geometry to that observed in nature (compare Figure 9d with Figure 6d or Figure 8a).

[41] The capture events and our earlier interpretations of Figures 7 and 8 are confirmed by the evolution of stream power of the major drainages through time as seen in Figure 9. At 6 Ma after initial collision most major drainages are developed (Figure 9b). The stream power is constant throughout the region (all rivers have the same color) as the starting uplift is easily balanced by the erosion rate at this stage. Discoloring at the model margin and in the Tarim Basin arise from boundary condition effects. With increasing uplift (Figure 9c at 29 Ma) erosion begins to lag behind uplift and in the regions of highest surface topography, the stream power increases (yellow sections of stream indicated by arrow in Figure 9c). During the Miocene uplift most of the model region does not experience changes in stream power: The entire region inside the uplifted region (geometry 4 in Figure 9a) increases in surface elevation, but gradients are not changed. At the margins of the uplifted region, stream power is increased substantially. This causes diversion of the Lower Yangtze from its SE course into a sharp knee, now flowing toward the NE (as indicated by the white arrow in Figure 9d). This corresponds very closely to its actual course in the eastern Tibetan Plateau where it changes its course from a southeastern to a northeastern orientation. Also, the uplift causes a relative base level lowering in the trailing edge of the syntaxis forming a knick point there (Figure 9d, gray arrow). This knick point causes rapid capture of several rivers formerly draining to the model boundary at "SE" by small streams now draining at "W." This may well correspond to the capture of the Yarlong-Tsangpo by the Brahmaputra at about the same time as the capture of the Lower Yangtze. Following the late uplift, small drainages (labeled with the black arrows in Figure 9d) bite into the new edge of the Plateau causing successive capture of the Middle Yangtze River. Ultimately, in the late Miocene stage shown in Figure 9e substantial parts of the Yangtze have been captured by northeast draining rivers. Similarly, the knick points of west draining rivers (meeting the model boundary at "w") rapidly migrate up river thereby increasing the region of high stream power.

5.4. Influence of Precipitation Contrasts

[42] The results presented above show that the first-order geometry of the drainages in and around the India-Asia collision zone can be predicted without considering the extreme precipitation contrasts documented across the range (Figure 10a). This is in part because we have not analyzed, explicitly, the difference between exhumation and erosion north and south of the Himalaya, but considered the orogen as a whole. However, we note that *Blythe et al.* [2007] recently suggested on the basis of a large set of fission track data now present for both sides of the Himalayan range that the rates of erosion appear to be largely independent of precipitation [see also *Burbank et al.*, 2003; *Thiede et al.*,

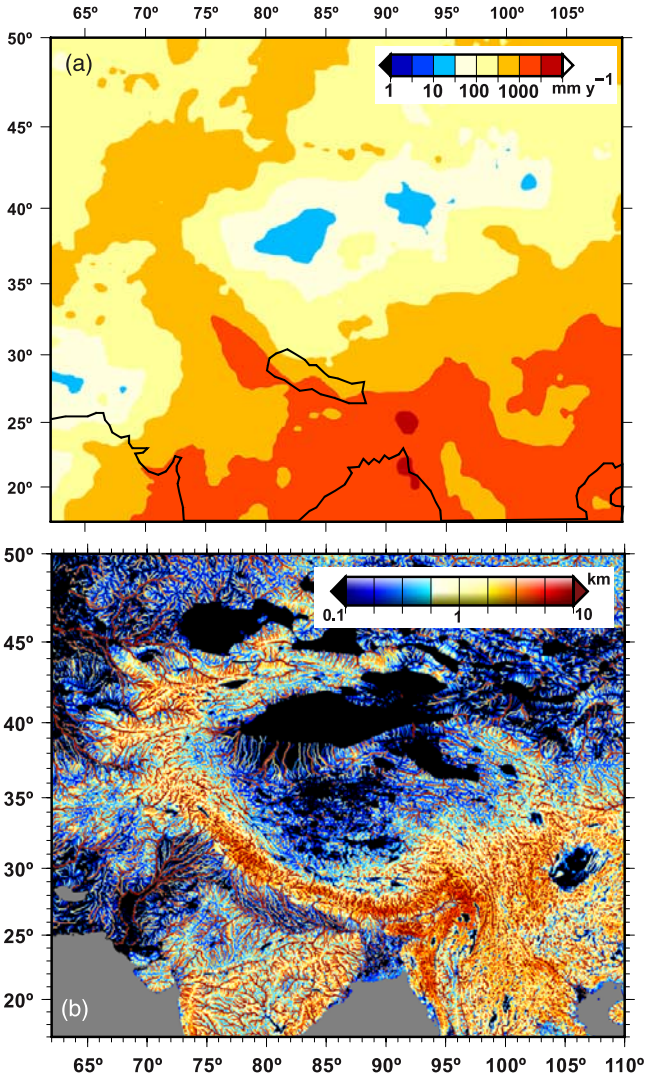

Figure 10. (a) Distribution of precipitation in the India-Asia collision zone (plotted from the Tropical Rainfall Measuring Mission (TRMM) data using Generic Mapping Tool). Indian coast and political boundary of Nepal are shown for reference. (b) Stream power map of the orogen considering precipitation contrasts using the refined definition of stream power from equation (8).

2005]. While *Blythe et al.* [2007] argued that this is due to the gradients of Himalayan rivers being above a threshold value, and may not be applicable to the entire orogen, their study illustrates that there is no consensus on the influence of climate on erosion rate. In order to test the influence of precipitation contrast on erosion we have recalculated the stream power distribution shown in Figure 7a using an improved formulation of precipitation-dependent stream power s_p, where

$$s_p = (p/p_m)^* A^{0.5}(dH/dL). \quad (8)$$

[43] There p is the local mean annual precipitation as derived from the TRMM data set and as shown in Figure 10a, and p_m is the mean annual precipitation averaged over the entire model region shown in Figure 10a. As such, Figure 10b may be directly compared with Figure 7a with higher and lower stream power values corresponding to higher or lower than mean precipitations. In comparison to Figure 7a, Figure 10b shows that (as may be expected from the distribution of rain fall) stream power values are much higher in the entire region south and east of the eastern syntaxis. This may influence our conclusion on the best fit erosion parameter. For the stream power differences between Figures 7a and 10b, there may be a variation of erosion parameter by 1 order of magnitude across the model region. Even an erosion parameter around $E = 50$ km^{-1} Ma^{-1} would maintain the surface elevation of the Tibetan Plateau as long as the Plateau remains arid. The capture events predicted here may occur in an even shorter time frame following the late uplift event when precipitation contrasts are considered.

6. Conclusion

[44] In summary we can conclude the following points:

[45] 1. The first-order geometry of the drainage network around the India-Asia collision zone is consistent with model results from an astonishingly simple model in which crustal thickening is driven by a hard indenter and erosion follows Hack's law. The model predicts that no displacement along major discontinuities is required to reproduce the first-order drainage pattern. A best fit for the observed drainage patterns is achieved with an erosion parameter around $E = 5$ km^{-1} Ma^{-1}.

[46] 2. A comparison of the stream power between model and nature shows that, in the model, stream power closely correlated with elevation and uplift rate. In contrast, in the India-Asia collision zone, stream power is a maximum in a ring shaped region that largely follows the margins off the Tibetan Plateau. Maximum regions are near the syntaxes.

[47] 3. Capture of Middle Yangtze River and subsequently the Upper Yangtze River drainages from its original course toward the southeast by the Lower Yangtze River draining through the Sichuan Basin toward the east is predicted by invoking a late uplift that encompasses the entire orogen, with a concave indentation in the region of the Sichuan Basin.

[48] 4. In our models, this late uplift also causes sufficient effective base level lowering in the Brahmaputra plains so that rapid head ward migration of the Brahmaputra causes capture of the Tsangpo.

[49] 5. Our results are largely independent of precipitation contrasts in the orogen.

[50] **Acknowledgments.** M. Clark, G. Houseman, J. Spotila, D. Burbank, and R. Gloaguen are thanked for reviews of an earlier version of this manuscript. This paper was written with the support of the Austrian Science Fund, projects P12864 and P19366.

References

Beaumont, C., R. A. Jamieson, M. H. Nguyen, and B. Lee (2001), Himalayan tectonics explained by extrusion of a low-viscosity crustal channel coupled to focused surface denudation, *Nature*, *414*, 738–742, doi:10.1038/414738a.

Blythe, A. E., D. W. Burbank, A. Carter, K. Schmidt, and J. Putkonen (2007), Plio-Quaternary exhumation history of the central Nepalese Himalaya: 1. Apatite and zircon fission track and apatite [U-Th]/He analyses, *Tectonics*, *26*, TC3002, doi:10.1029/2006TC001990.

Bookhagen, B., and D. W. Burbank (2006), Topography, relief, and TRMM-derived rainfall variations along the Himalaya, *Geophys. Res. Lett.*, *33*, L08405, doi:10.1029/2006GL026037.

Bookhagen, B., R. C. Thiede, and M. R. Strecker (2005), Abnormal monsoon years and their control on erosion and sediment flux in the high, arid northwest Himalaya, *Earth Planet. Sci. Lett.*, *231*, 131–146, doi:10.1016/j.epsl.2004.11.014.

Braun, J., and M. Sambridge (1997), Modelling landscape evolution on geological time scales: A new method based on irregular spatial discretization, *Basin Res.*, *9*, 27–52, doi:10.1046/j.1365-2117.1997.00030.x.

Brookfield, M. E. (1998), The evolution of the great river systems of southern Asia during the Cenozoic India-Asia collision: Rivers draining southwards, *Geomorphology*, *22*, 285–312, doi:10.1016/S0169-555X(97)00082-2.

Burbank, D. W., A. E. Blythe, J. Putkonen, B. Pratt-Sitaula, E. Gabet, M. Oskin, A. Barros, and T. Ohja (2003), Decoupling of erosion and precipitation in the Himalayas, *Nature*, *426*, 652–655, doi:10.1038/nature02187.

Burchfiel, B. C., Z. Chen, Y. Liu, and L. H. Royden (1995), Tectonics of the Longmen Shan and adjacent regions, Central China, *Int. Geol. Rev.*, *37*, 661–735.

Clark, M. K., and L. H. Royden (2000), Topographic ooze: Building the eastern margin of Tibet by lower crustal flow, *Geology*, *28*, 703–706, doi:10.1130/0091-7613(2000)28<703:TOBTEM>2.0.CO;2.

Clark, M. K., L. M. Schoenbohm, L. H. Royden, K. X. Whipple, B. C. Burchfiel, X. Zhang, W. Tang, E. Wang, and L. Chen (2004), Surface uplift, tectonics, and erosion of eastern Tibet from large-scale drainage patterns, *Tectonics*, *23*, TC1006, doi:10.1029/2002TC001402.

Clark, M. K., M. A. House, L. H. Royden, K. X. Whipple, B. C. Burchfiel, X. Zhang, and W. Tang (2005a), Late Cenozoic uplift of southeastern Tibet, *Geology*, *33*, 525–528, doi:10.1130/G21265.1.

Clark, M. K., J. W. M. Bush, and L. H. Royden (2005b), Dynamic topography produced by lower crustal flow against rheological strength heterogeneities bordering the Tibetan Plateau, *Geophys. J. Int.*, *162*, 575–590, doi:10.1111/j.1365-246X.2005.02580.x.

Clark, M. K., L. H. Royden, K. X. Whipple, B. C. Burchfiel, X. Zhang, and W. Tang (2006), Use of a regional, relict landscape to measure vertical deformation of the eastern Tibetan Plateau, *J. Geophys. Res.*, *111*, F03002, doi:10.1029/2005JF000294.

England, P. C., and G. A. Houseman (1986), Finite strain calculations of continental deformation: 2. Comparison with the India-Asia collision zone, *J. Geophys. Res.*, *91*, 3664–3676, doi:10.1029/JB091iB03p03664.

England, P. C., and G. A. Houseman (1988), The mechanics of the Tibetan Plateau, *Philos. Trans. R. Soc. Ser. A*, *326*, 301–320, doi:10.1098/rsta.1988.0089.

England, P. C., and D. P. McKenzie (1982), A thin viscous sheet model for continental deformation, *Geophys. J. R. Astron. Soc.*, *70*, 295–321.

Enkelmann, E., L. Ratschbacher, R. Jonckheere, R. Nestler, M. Fleischer, R. Gloaguen, B. R. Hacker, Y. Q. Zhang, and Y. S. Ma (2006), Cenozoic exhumation and deformation of northeastern Tibet and the Qinling: Is Tibetan lower crustal flow diverging around the Sichuan Basin?, *Geol. Soc. Am. Bull.*, *118*, 651–671, doi:10.1130/B25805.1.

Hack, J. T. (1957), Studies of longitudinal profiles in Virginia and Maryland, *U. S. Geol. Surv. Prof. Pap., 294-B*.

Hallet, B., and P. Molnar (2001), Distorted drainage basins as markers of crustal strain east of the Himalaya, *J. Geophys. Res.*, *106*, 13,697–13,709, doi:10.1029/2000JB900335.

Harrison, T. M., P. Copeland, W. S. F. Kidd, and A. Yin (1992), Raising Tibet, *Science*, *255*, 1663–1670, doi:10.1126/science.255.5052.1663.

Hergarten, S. (2002), *Self-Organized Criticality in Earth Systems*, 272 pp., Springer, New York.

Hergarten, S., C. Roffeis, and K. Stüwe (2006), The search for tectonic signatures in river profiles in the Styrian Basin, *Geophys. Res. Abstr.*, *8*, 04421, SRef-ID:1607-7962/gra/EGU06-A-04421.

Hodges, K. V. (2000), Tectonics of the Himalaya and southern Tibet from two perspectives, *Geol. Soc. Am. Bull.*, *112*, 324–350, doi:10.1130/0016-7606(2000)112<0324:TOTHAS>2.3.CO;2.

Houseman, G. A., and P. C. England (1986), Finite strain calculations of continental deformation: 1. Method and general results for convergent zones, *J. Geophys. Res.*, *91*, 3651–3663, doi:10.1029/JB091iB03p03651.

Houseman, G. A., and P. C. England (1993), Crustal thickening versus lateral expulsion in the India-Asia continental collision, *J. Geophys. Res.*, *98*, 12,233–12,249, doi:10.1029/93JB00443.

Houseman, G. A., and P. C. England (1996), A crustal thickening model for the Indo-Asian collision, in *Tectonic Evolution of Asia*, edited by A. Yin and T. M. Harrison, pp. 1–17, Cambridge Univ. Press, New York.

Lee, T. T., and L. A. Lawver (1995), Cenozoic plate reconstruction of Southeast Asia, *Tectonophysics*, *251*, 85–138, doi:10.1016/0040-1951(95)00023-2.

Massonne, H.-J., and P. J. O'Brien (2003), The Bohemian Massif and the NW Himalaya, in *Ultrahigh Pressure Metamorphism*, *Notes Mineral.*, vol. 5, edited by D. A. Carswell and R. Compagoni, pp. 145–187, Eur. Mineral. Union, Wien, Austria.

Miller, S. R., R. L. Slingerland, and E. Kirby (2002), Landscape evolution in orogens with significant lateral advection of rock: Insights from numerical simulations of fault-bend folds, *Eos Trans. AGU*, *83*(47), Fall Meet. Suppl., Abstract T72B-05.

Molnar, P., and H. Lyon-Caen (1988), Some simple physical aspects of the support, structure, and evolution of mountain belts, *Spec. Pap. Geol. Soc. Am.*, *218*, 179–207.

Montgomery, D. R. (1994), Valley incision and the uplift of mountain peaks, *J. Geophys. Res.*, *99*, 13,913–13,921, doi:10.1029/94JB00122.

Montgomery, D. R., and D. B. Stolar (2006), Reconsidering Himalayan river anticlines, *Geomorphology*, *82*, 4–15, doi:10.1016/j.geomorph.2005.08.021.

Neil, E. A., and G. A. Houseman (1997), Geodynamics of the Tarim Basin and the Tien Shan in central Asia, *Tectonics*, *16*, 571–584, doi:10.1029/97TC01413.

Nelson, K. D., et al. (1996), Partially molten middle crust beneath southern Tibet: Synthesis of Project INDEPTH results, *Science*, *274*, 1684–1687, doi:10.1126/science.274.5293.1684.

Oberlander, T. M. (1985), Origin of drainage transverse to structures in orogens, in *Tectonic Geomorphology*, edited by M. Morisawa and J. T. Hack, pp. 155–182, Allen and Unwin, Boston.

Robl, J., and K. Stüwe (2005), Continental collision with finite indenter strength: 2. European Eastern Alps, *Tectonics*, *24*, TC4014, doi:10.1029/2004TC001741.

Robl, J., K. Stüwe, and S. Hergarten (2008), Channel profiles around Himalayan river anticlines: Constraints on their formation from digital elevation model analysis, *Tectonics*, *27*, TC3010, doi:10.1029/2007TC002215.

Rowley, D. B., and B. S. Currie (2006), Palaeo-altimetry of the late Eocene to Miocene Lunpola basin, central Tibet, *Nature*, *439*(9), 677–681, doi:10.1038/nature04506.

Royden, L. H. (1996), Coupling and decoupling of crust and mantle in convergent orogens: Implications for strain partitioning in the crust, *J. Geophys. Res.*, *101*, 17,679–17,705, doi:10.1029/96JB00951.

Schoenbohm, L. M., B. C. Burchfiel, L. Chen, and J. Yin (2006a), Miocene to present activity along the Red River Fault, China in the context of continental extrusion, upper crustal rotation, and lower-crustal flow, *Geol. Soc. Am. Bull.*, *118*, 672–688, doi:10.1130/B25816.1.

Schoenbohm, L. M., B. C. Burchfiel, and C. Liangzhong (2006b), Propagation of surface uplift, lower crustal flow, and Cenozoic tectonics of the southeast margin in the Tibetan Plateau, *Geology*, *34*, 813–816, doi:10.1130/G22679.1.

Seeber, L., and V. Gornitz (1983), River profiles along the Himalayan Arc as indicators of active tectonics, *Tectonophysics*, *92*, 335–367, doi:10.1016/0040-1951(83)90201-9.

Shapiro, N. M., M. H. Ritzwoller, P. Molnar, and V. Levin (2004), Thinning and flow of Tibetan Crust constrained by seismic anisotropy, *Science*, *305*, 233–236, doi:10.1126/science.1098276.

Spicer, R., N. Harris, M. Widdowson, A. Herman, S. Guo, P. Valdes, J. Wolfe, and S. Kelley (2003), Constant elevation of southern Tibet over the past 15 million years, *Nature*, *421*, 622–624, doi:10.1038/nature01356.

Stüwe, K. (2007), *Geodynamics of the Lithosphere: An Introduction*, 495 pp., Springer, New York.

Tapponnier, P., Z. Xu, F. Roger, B. Meyer, N. Arnaud, G. Wittlinger, and Y. Jingsui (2001), Oblique stepwise rise and growth of the Tibet Plateau, *Science*, *294*, 1671–1677, doi:10.1126/science.105978.

Tenczer, V., K. Stüwe, and T. Barr (2001), Pressure anomalies around cylindrical objects in simple shear, *J. Struct. Geol.*, *23*, 777–788, doi:10.1016/S0191-8141(00)00155-3.

Thiede, R., J. R. Arrowsmith, B. Bookhagen, M. O. McWilliams, E. Sobel, and M. Strecker (2005), From tectonically to erosionally controlled development of the Himalayan orogen, *Geology*, *33*, 689–692, doi:10.1130/G21483.1.

Treloar, P. J., P. J. O'Brian, R. R. Parrish, and M. A. Khan (2003), Exhumation of early Tertiary coesite bearing eclogites from the Pakistan Himalaya, *J. Geol. Soc.*, *160*, 367–376.

Vannay, J. C., B. Grasemann, M. Rahn, W. Frank, A. Carter, V. Baudraz, and M. Cosca (2004), Miocene to Holocene exhumation of metamorphic crustal wedges in the NW Himalaya: Evidence for tectonic extrusion coupled to fluvial erosion, *Tectonics*, *23*, TC1014, doi:10.1029/2002TC001429.

Whipple, K. X., and G. E. Tucker (1999), Dynamics of stream power river incision model: Implications for height limits of mountain ranges, landscape response time scales and research needs, *J. Geophys. Res.*, *104*, 17,661–17,674, doi:10.1029/1999JB900120.

Willett, S. D., N. Hovius, and R. Slingerland (1999), The effects of horizontal motion on topography and patterns of exhumation in convergent mountain belts, *Eos Trans. AGU*, *80*(46), F1033.

Wobus, C., K. X. Whipple, E. Kirkby, N. Snyder, J. Johnson, K. Spyropolou, B. T. Crosby, and

D. Sheehan (2006), Tectonics from topography: Procedures, promise and pitfalls, in *Tectonics*, *Climate, and Landscape Evolution*, edited by S. Willett, *Spec. Pap. Geol. Soc. Am.*, *398*, 55–74.

Zeitler, P. K., A. S. Meltzer, P. O. Koons, B. Hallet, C. P. Chamberlain, W. S. F. Kidd, S. K. Park, L. Seeber, M. Bishop, and J. Shroder (2001), Erosion, Himalayan geodynamics, and the geomorphology of metamorphism, *GSA Today*, *11*, 4–9, doi:10.1130/1052-5173(2001)011<0004:EHGATG>2.0.CO;2.

Zhang, P.-Z., et al. (2004), Continuous deformation of the Tibetan Plateau from global positioning system data, *Geology*, *32*, 809–812, doi:10.1130/G20554.1.

L. Evans, S. Hergarten, J. Robl, and K. Stüwe, Department of Earth Science, University of Graz, Heinrichstrasse 26, A-8010 Graz, Austria. (kurt.stuewe@uni-graz.at)